Bull. Mater. Sci., Vol. 39, No. 3, June 2016, pp. 777–788. © Indian Academy of Sciences.
DOI 10.1007/s12034-016-1203-1

Effect of europium content on physical properties of In_2O_3 thin films for sensitivity and optoelectronic applications

O KAMOUN[1], A BOUKHACHEM[1,*], C MRABET[1], A YUMAK[2], P PETKOVA[3], K BOUBAKER[1] and M AMLOUK[1]

[1]Unité de Physique des Dispositifs à Semi-conducteurs, Faculté des Sciences de Tunis, Université de Tunis El Manar, 2092 Tunis, Tunisia
[2]Physics Department, Faculty of Arts and Sciences, Marmara University, 34722 Istanbul, Turkey
[3]Shumen University, 'Konstantin Preslavsky', 9712 Shumen, Bulgaria

MS received 2 November 2015; accepted 15 December 2015

Abstract. **In_2O_3 : Eu thin films were successfully grown by spray pyrolysis. XRD studies showed that the films had In_2O_3 cubic structure with (004) preferential orientation and best crystal properties at 1.5% Eu doping level. The optical band gap energy decreased with Eu content around 4.1 eV. Urbach energy was of the order of 278 meV, it decreased with Eu content which indicates a decrease in the defects by doping. The dispersion of the refractive index was discussed. Raman spectroscopy showed the band positions corresponding to In_2O_3 cubic phase with a small shift related to europium incorporation within In_2O_3 matrix. PL measurements showed a large band which was located at 410 nm and related to the band-to-band transitions and other bands related to impurity levels. Finally, the electric conductivity was investigated depending on the effect of temperature. Activation energy was found to range from 45 to 60 meV for films which were prepared with 1% Eu content.**

Keywords. **Indium oxide; europium doping; Raman spectroscopy; PL measurement; electrical behaviour.**

1. Introduction

Indium oxides (In_2O_3) have particular optical and electronic properties [1–3] which can be of interest for electronic and optoelectronic devices [4,5]. They are also important in selective oxidation catalysis [6–8]. This interesting material was found in many works for its interesting properties particularly its high thermal and chemical stabilities.

It has been recorded that indium oxide is a cubic-structured semiconductor with high piezoelectric and gas detection properties [9–16]. Its deposition on glass-like substrates has been widely experimented and applied.

To improve physical properties of In_2O_3, it was doped by several elements such as tin [17,18], zirconium [19] and manganese [20]. Although this oxide was doped by several other elements, very few of these studies have been reported on rare-earth doping.

In_2O_3 thin films were prepared by many techniques such as MOCVD [21], chemical vapour transport (CVT) [22], sputtering [23], laser ablation [24], spray pyrolysis [25] and sol–gel [26,27]. Compared to other techniques, spray pyrolysis method is widely used to prepare indium oxide thin films. In_2O_3 samples are also characterized by uniform size distribution and it has been shown that thin films with grain size were controlled through doping concentration. Furthermore, spray pyrolysis technique leads to a large production area and it is special to give crystallized thin films without recourse to thermal processing [25].

In this work, our aims are to study the effect of europium content $\left(y = \left[Eu^{3+}\right]/\left[In^{3+}\right], 0 \leq y \leq 2\ \text{at}\%\right)$ on the structural, electrical and optical properties of In_2O_3 : Eu thin films. These films have been investigated by XRD, optical reflectance, transmission spectra, PL and Raman spectroscopy. On the other hand, an attempt on their electrical properties has been carried out by means of conductivity measurements alteration in terms of temperature.

2. Experimental

2.1 *In_2O_3 : Eu films preparation*

Indium oxide thin films were deposited on glass substrates at 460°C using 0.01 M aqueous solution of indium (III) chloride tetrahydrate [$InCl_3 \cdot 4H_2O$]. Nitrogen was used as the carrier gas (pressure at 0.35 bar) through a 0.5 mm diameter nozzle. As reported in our laboratory [28], the nozzle-to-substrate plane distance was fixed at the optimal value of 27 cm. During the deposition process, the precursor mixture flow rate was taken constantly at 4 ml min^{-1}.

Under similar experimental conditions, europium-doped In_2O_3 : Eu thin film solutions have been fabricated by adding europium oxide to precursor solutions, while maintaining acidity level. In the elaborated samples, the europium-to-indium molar ratios $y = \left[Eu^{3+}\right]/\left[In^{3+}\right]$ were 0.5; 1; 1.5 and 2%.

*Author for correspondence (abdelwaheb.boukhachem@laposte.net)

2.2 *Characterization techniques*

The structural analysis of obtained thin films was carried out using X-ray apparatus (Philips PW 1729 system) using CuKα monochromatic radiation ($\lambda = 0.15405$ nm). The optical transmittance T (λ) and reflectance R (λ) of In_2O_3 : Eu spray thin films were recorded using a Perkin Elmer Lambda 950 spectrophotometer in a 300–1800 nm wavelength domain. Raman spectroscopy and PL measurement of In_2O_3 : Eu sprayed thin films were carried out by using Jobin Yron and Perkin Elmer LS55 equipments, respectively.

Finally, electrical conductivity measurements of In_2O_3 : Eu thin film have been performed using four probe method at different temperature (figure 1). Photocatalytic properties of In_2O_3 : Eu ($0 \leq y \leq 6$ at%) were also studied.

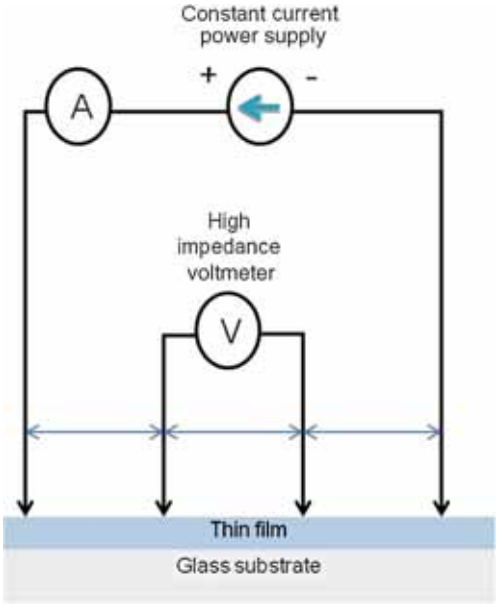

Figure 1. Configuration of Four probe method for the electrical measurements.

3. Results and discussion

3.1 *Structural analyses*

The X-ray diffraction spectra of europium-doped indium oxide thin films are reported in figure 2. It shows the effect of concentrations ratios of europium and indium ions in the spray solution ($y = [Eu^{3+}]/[In^{3+}]$, $0 \leq y \leq 2$ at%). The observed XRD pattern is found to match with JCPDS card 06-0416.

With further increase of europium concentration until 1.5 at%, a sharp and intense (004) peak is obtained that corresponds to enhancement of crystal quality. When europium content is higher than 1.5 at%, the intensity of (004) peak decreases to the detriment of the increase of (222) intensity. For europium inclusion equal to 1.5 at%, we remark the presence of new peak at 2θ equal to 31.7° corresponding to Eu_3O_4 orthorhombic phase oriented on to (211) direction.

The texture coefficient (TC) which indicates the maximum preferred orientation of the films along the diffraction plane means that the increase in the preferred orientation is associated with increase in the number of grains along that plane. $TC_{(hkl)}$ values have been calculated from X-ray data, using the following equation [29–34]:

$$TC_{(hkl)} = \frac{I(hkl)/I_0(hkl)}{N^{-1}\sum I(hkl)/I_0(hkl)}, \quad (1)$$

where $I(hkl)$ is the measured relative intensity of (hkl) plane, $I_0(hkl)$ the standard intensity of the same plane taken from the JCPDS card 06-0416 and N the reflection number. $TC_{(hkl)}$ calculated values of the doped In_2O_3 thin films are given in table 1.

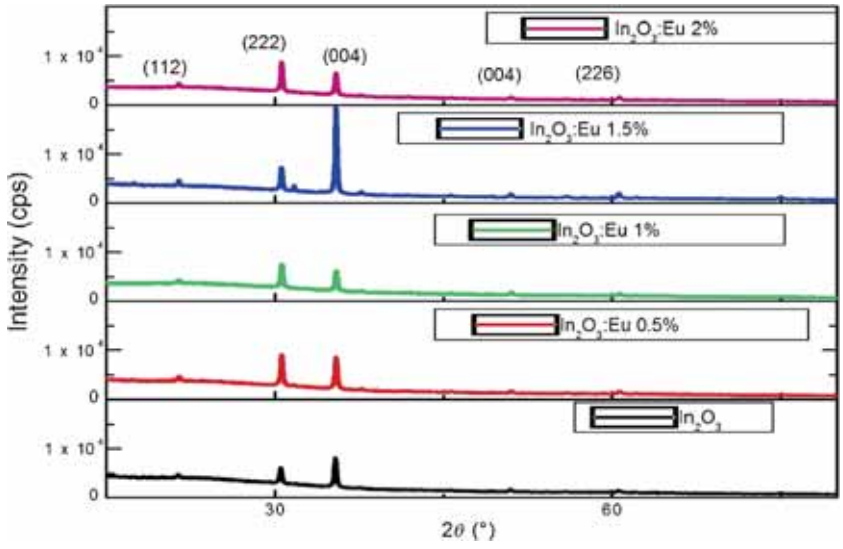

Figure 2. X-ray diffraction spectra of Eu-doped In_2O_3 thin films for different ratios in the spray solution.

Table 1. Texture coefficient $TC_{(hkl)}$ values of Eu-doped In_2O_3 spayed thin films.

	TC				
$y = [Eu^{3+}]/[In^{3+}]$ at%	0	0.5	1	1.5	2
TC(112)	0.685	1.011	0.927	0.573	1.118
TC(222)	0.516	0.801	0.852	0.288	0.996
TC(004)	3.269	2.726	2.557	3.755	2.451
TC(044)	0.252	0.181	0.287	0.131	0.198
TC(226)	0.275	0.278	0.374	0.251	0.235

Table 2. Lattice parameters of In_2O_3 : Eu thin films.

$y = [Eu^{3+}]/[In^{3+}]$ at%	0	0.5	1	1.5	2
a (Å)	10.1423	10.1423	10.1277	10.1277	10.1314

All the XRD reflections can be indexed to the cubic In_2O_3, no other peaks can be observed, revealing their phase is pure cubic structures. The interplanar spacing d_{hkl} values were calculated by using Bragg equation [30,32]:

$$2d_{hkl} \sin\theta = n\lambda, \tag{2}$$

where n is the order of diffraction (usually $n = 1$) and λ the X-ray wavelength.

In the cubic structure, the plane spacing is related to the lattice constant a and the Miller indices (hkl) by the following relation [33]:

$$d_{hkl} = \frac{a}{\sqrt{h^2 + k^2 + l^2}}. \tag{3}$$

The lattice parameter a of In_2O_3 : Eu is given in table 2.

From calculated values of lattice parameter listed in table 2, it is found that this parameter reaches a low value for 1% Eu content. This value seems to be an appropriate value for possible incorporation of this doping inside the indium oxide thin film. Also, when Eu content increases, this parameter also increases, showing a possible escape of this doping element to form oxides with high index such as Eu_2O_3. The latest has a crystalline phase different to cubic structure and goes with the structural and optical properties described above. Indeed, the compactness of the host material increases at this special doping and induces a high photon interaction of this 1% Eu-doped In_2O_3 oxide.

The average grain size D of indium oxide calculated from (112), (222), (004), (044) and (226) diffraction peaks using Sherrer's formula [34,35] are listed in table 3.

$$D = \frac{k\lambda}{\beta_{1/2} \cos(\theta)}, \tag{4}$$

where $k = 0.9$ is the Sherrer constant, $\lambda = 1.54$ Å the wavelength of CuKα radiation, $\beta_{1/2}$ the full-width at half-maximum of each peaks and θ the Bragg angle. The grain size was found to range from 24.4 to 53.4 nm when the concentration of Eu varies from 0 to 2 at%. We note that the larger size of the crystallite is obtained for europium rate equal to 1.5 at%. Then, we can conclude that the best crystallinity of In_2O_3 : Eu is obtained for Europium content equal to 1.5 at%.

Table 3. Grain size of Eu-doped In_2O_3 thin films using different XRD peaks.

	D (nm)				
$y = [Eu^{3+}]/[In^{3+}]$ at%	0	0.5	1	1.5	2
D(112)	33.2	42.8	42.6	53.4	46.7
D(222)	34.9	38.9	36.0	51.3	44.3
D(004)	36.3	35.6	3.6	49.5	39.2
D(044)	41.6	28.1	37.4	41.9	24.5
D(226)	36.9	33.6	39.0	46.8	29.8

Table 4. Microstrain of Eu-doped In_2O_3 thin films.

	ξ (10^{-3})				
$y = [Eu^{3+}]/[In^{3+}]$ at%	0	0.5	1	1.5	2
ξ(112)	11.19	8.65	8.70	6.94	7.93
ξ(222)	7.49	6.70	7.24	5.08	5.89
ξ(004)	6.21	6.32	5.83	4.55	5.75
ξ(044)	3.78	5.59	4.20	3.75	6.45
ξ(226)	3.60	3.94	3.40	2.83	4.44

Table 5. Dislocation density of Eu-doped In_2O_3 thin films.

	δ (10^{14} line m^{-2})				
$y = [Eu^{3+}]/[In^{3+}]$ at%	0	0.5	1	1.5	2
D(112)	9.07	5.46	5.51	3.51	9.07
D(222)	8.21	6.61	7.72	3.80	8.21
D(004)	7.59	7.89	771.60	4.08	7.59
D(044)	5.78	12.66	7.15	5.70	5.78
D(226)	7.34	8.86	6.57	4.57	7.34

The microstrain ξ, which is an interesting structural parameter of In_2O_3 : Eu sprayed-thin films is calculated using the following relation [36,37]:

$$\xi = \frac{\beta_{1/2}}{4 \tan(\theta)}. \tag{5}$$

All results are listed in table 4. From these results, we conclude that ξ decreases uniformly when y is from 0 to 1.5 at%. While for (004), direction decreases. ξ decreases from 7.49 ($y = 0\%$) to 5.08 ($y = 1.5\%$) and from 6.21 ($y = 0\%$) to 4.55 ($y = 1.5\%$), respectively, for (222) and (004) planes. For all (hkl) planes, the smallest values of ξ are obtained for Eu content equal to 1.5 at%.

Using grain size values (table 5), the dislocation density δ_{dis} defined as the imperfection in crystal has been calculated using the Williamson and Smallman's formula [38]:

$$\delta_{dis} = \frac{1}{D^2}. \tag{6}$$

The dislocation density values listed in table 5 confirm the effect of europium incorporation in In_2O_3 matrix. Indeed, a maximum value of this structural parameter is obtained at 1% Eu doping level. This may be due to nanosize crystallites (table 3) character of such doped film.

The probability made for the texture coefficient is for a given orientation; it can be used to calculate the averages of crystallite size D and microstrain ξ and can thus outperform the Williamson and Hall relationship [10,11] using:

$$D_{\text{moy}} = \frac{\sum \text{TC}_{(hkl)}.D_{(hkl)}}{\sum \text{TC}_{(hkl)}}, \tag{7}$$

$$\xi_{\text{moy}} = \frac{\sum \text{TC}_{(hkl)} \cdot \xi_{(hkl)}}{\sum \text{TC}_{(hkl)}}. \tag{8}$$

Likewise, the average value of dislocation density can be estimated using a similar formula:

$$\delta_{\text{moy}} = \frac{\sum \text{TC}_{(hkl)} \cdot \delta_{(hkl)}}{\sum \text{TC}_{(hkl)}}. \tag{9}$$

Average values of crystallite size, stress and dislocation density are given in table 6, from which we can conclude that the biggest crystal size ($D_{\text{moy}} = 49.7$ nm) and the smallest values of dislocation density ($\delta_{\text{moy}} = 5.4\times10^{14}$ lines m^{-2}) and microstrain ($\xi_{\text{moy}} = 5.6\times10^{-3}$) are obtained for Eu content $y = 1.5$ at%. From this structural analysis, we can confirm that a clear improvement of In_2O_3 crystallinity is obtained for ratio between europium and indium concentrations in the spray solution equal to 1.5 at%

$$\left(y = \frac{[\text{Eu}^{3+}]}{[\text{In}^{3+}]} = 1.5 \text{ at\%}\right).$$

On the other hand, SEM observations provided by Philips apparatus allow us to get microscopic information of the surface structure when Eu content increases. Indeed, these micrographs (figure 3) reveal that all film surfaces are rough. These perturbed surfaces are probably due to very small droplets resulting from the spray pyrolysis technique that vaporize above the glass substrates and condense as microcrystallites with various dimensions (50–200 nm).

Table 6. Average values of grain size, dislocation density and microstrain of In_2O_3 : Eu thin films.

	D_{avr} (nm)	δ_{moy} (10^{14} lines m^{-2})	ξ_{moy} ($\times10^{-3}$)
In_2O_3	36.02	7.6	6.76
In_2O_3 : Eu 0.5%	37.20	7.4	6.69
In_2O_3 : Eu 1%	38.86	6.7	6.33
In_2O_3 : Eu 1.5%	49.7	5.4	5.60
In_2O_3 : Eu 2%	40.83	6.4	6.22

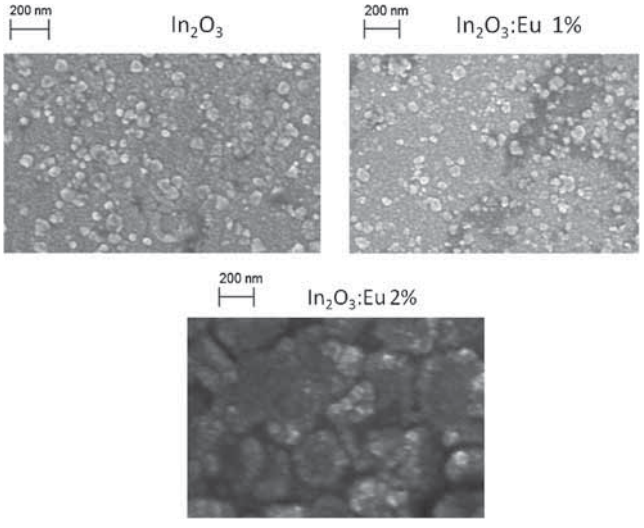

Figure 3. SEM observations of Eu-doped In_2O_3 thin films.

3.2 *Optical properties of crystalline In_2O_3 : Eu thin films*

3.2a *Reflectance and transmission spectra*: The optical transmission spectrum of the Eu-doped In_2O_3 thin film grown on glass substrates is shown in figure 4. The average

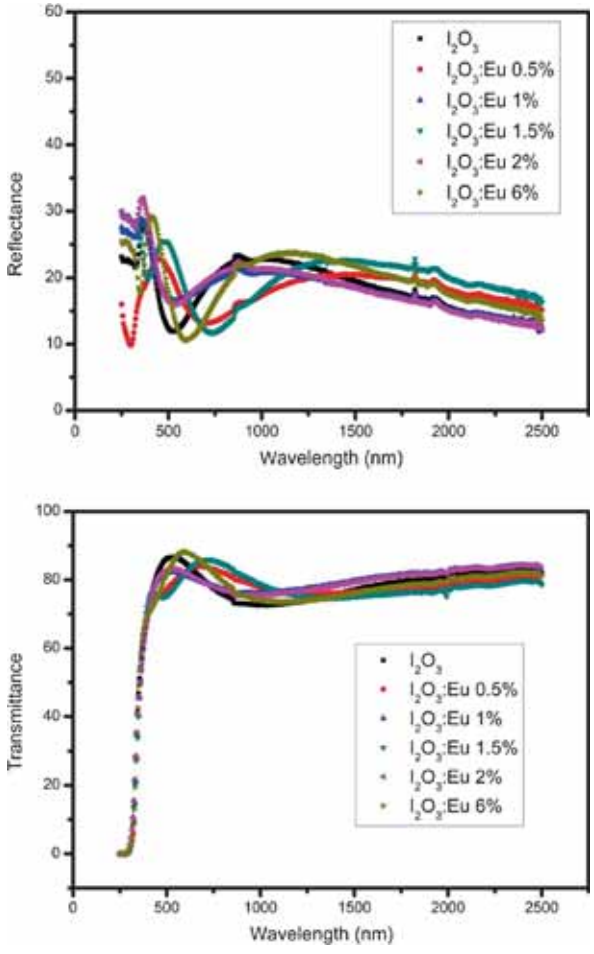

Figure 4. Reflection and transmission spectra of Eu-doped In_2O_3 thin films.

value of transmittance in the visible range is found to be 70–85%, while the reflectance remains inside a narrow interval (10–30%). In the visible region of solar spectrum, both reflectance and transmission spectra show the presence of the interference phenomenon indicates a smooth and homogeneous surface of all observed films [39].

3.2b *Effect of Eu content on the absorption and optical band gap*: The absorption coefficient α of prepared thin films was determined from transmittance (T) measurements using the following expression [40]:

$$\alpha = \frac{1}{d}\ln\frac{1}{T}, \tag{10}$$

where d is the film thickness.

The optical absorption edge was analysed by the following equation:

$$\alpha h\nu = B(h\nu - E_g)^p, \tag{11}$$

where B is a constant, E_g the band-gap energy of the corresponding material, p a number which have the value of 1/2 or 2 for direct transition and indirect ones, respectively. In figure 5, we reported $(\alpha h\nu)^2$ as a function of incident photon energy ($h\nu$).

It has been observed that the plots of $(\alpha h\nu)^2$ *vs.* $h\nu$ were linear over a wide range of photon energies indicating that it is a direct transition. The intercept (extrapolation) of this plot (straight line) on the energy axis give the energy band gap whose values are shown in table 7. This table shows a dependency of band gap energy with the Eu content.

This phenomenon may be related to the europium incorporation into In_2O_3 matrix. It is found that a minimum value of band gap ($E_g = 4.09$ eV) for 1.5% doping level.

On the other hand, the defects on the prepared thin films suggested above are interpreted by the spreading of state densities in the band gap, it is performed by the empirical Urbach model, which stipulates that the absorption coefficient follows the law:

$$\alpha = \alpha_0 \exp\left(\frac{h\nu}{E_U}\right), \tag{12}$$

where α_0 is a constant and E_U the Urbach energy which characterizes the slope of the exponential limit (figure 6). The value of E_U is obtained from the inverse of the slope of $\ln\alpha$ *vs.* $h\nu$ [37] using the following relation and are given in table 7:

$$E_U = \left[\frac{d\ \ln\alpha}{dh\nu}\right]^{-1}. \tag{13}$$

For Eu-doped indium oxide thin film, the Urbach energy changes with the concentration of doping. This suggests that defects and impurities from interstitial indium atom disappear depending on the doping concentration. Thus, the dopant causes a reorganization of the structure as shown in figure 2, that the best crystallinity is obtained for $y = [Eu^{3+}]/[In^{3+}] = 1.5$ at%. This result is consistent with other; i.e., Mott and Davis [41]. Note that unlike crystalline structures in the fundamental edge are mainly determined by conduction and valence levels, ion-doped binary semiconductor compounds present a particular optical absorption edge profile. In these materials, the absorption coefficient profile increases exponentially with the photon energy near the energy gap. This variation results in 'blurring' of the valence-conduction bands and slightly narrows the band gap by appearance of the so-called Urbach tailing.

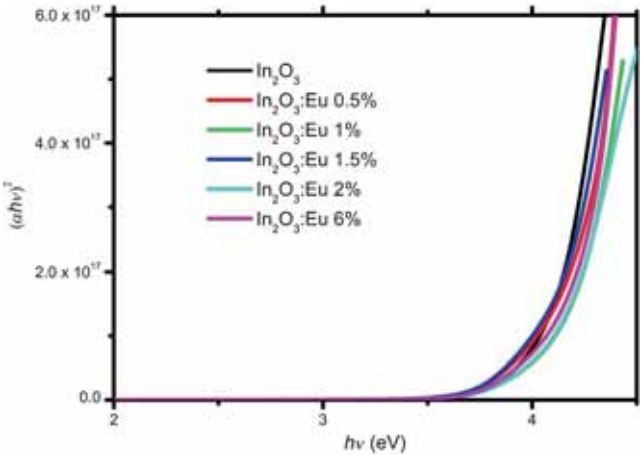

Figure 5. $(\alpha h\nu)^2$ and $\ln(\alpha)$ *vs.* $h\nu$ for Eu-doped In_2O_3 thin films.

Table 7. Urbach and band gap energies of Eu-doped In_2O_3 thin films.

	E_U (meV)	E_g (eV)
In_2O_3	278	4.10
In_2O_3 : Eu 0.5%	285	4.17
In_2O_3 : Eu 1%	313	4.15
In_2O_3 : Eu 1.5%	289	4.09
In_2O_3 : Eu 2%	309	4.10

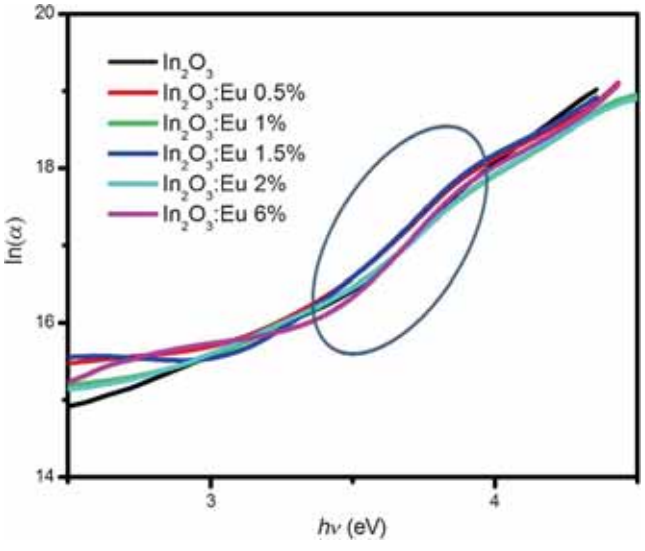

Figure 6. Plots of $\ln(\alpha)$ *vs.* $h\nu$.

3.2c *Refractive index and extinction coefficient*: The refractive index and extinction coefficient are the most important parameters of optical materials and their applications. Thus, it is important to determine these two optical parameters of the deposited thin films. The optical characteristics of dispersion $n(\lambda)$ and $k(\lambda)$ (refractive index and extinction coefficient, respectively), for values of the wavelength λ between 300 and 1800 nm, have been calculated using optical experimental measurements and the method of Bathe *et al* [42] and Belgacem *et al* [43]. The present research is based on the resolution of the following system of nonlinear equations:

$$\begin{cases} R_{\text{exp}}(n,k,\lambda) - R_{\text{theo}}(n,k,\lambda) = 0, \\ T_{\text{exp}}(n,k,\lambda) - T_{\text{theo}}(n,k,\lambda) = 0. \end{cases} \quad (14)$$

R_{theo} and R_{exp} represent, respectively, the theoretical and experimental reflectance and, T_{theo} and T_{exp} represent, respectively, the theoretical and experimental transmittance. The plots of $n(\lambda)$ and $k(\lambda)$ are presented in figure 7. It is found that the refractive index has hyperbolic decreases as a function of wavelength. This evolution is modelled by the Cauchy law [36]:

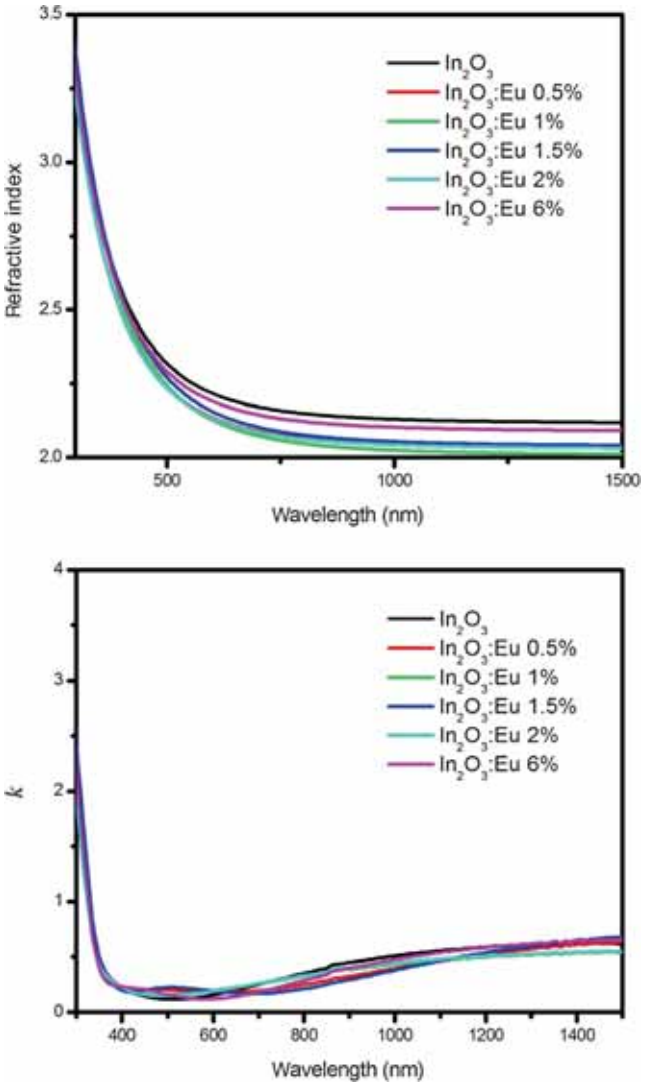

Figure 7. Refractive index and extinction coefficient of Eu-doped In_2O_3 thin films.

Table 8. Optical constants of Cauchy law and E_0 and E_d energies.

	A	B (nm^2)	E_0 (eV)	E_d (eV)
In_2O_3	2.10186	30237.621	4.797	15.544
In_2O_3 : Eu 0.5%	2.01738	31786.7837	4.720	13.910
In_2O_3 : Eu 1%	1.99072	38332.1511	4.451	12.412
In_2O_3 : Eu 1.5%	2.02063	37649.292	4.509	13.159
In_2O_3 : Eu 2%	2.01489	31302.3442	4.749	13.593

$$n = A + \frac{B}{\lambda^2}, \quad (15)$$

where A and B are the Cauchy's parameters and λ is the wavelength of the light used, implying that the films have normal dispersion along the entire studied range of wavelength. A and B values for In_2O_3 : Eu-sprayed thin films are given in table 8. In addition to the Cauchy extrapolation described above, which was done to provide reasonable values for refractive index in the spectral range of low absorption, we have also carried out some other optical constants based on Wemple–DiDomenico single-oscillator model. In fact, in the band of low absorption, we can approximate n^2 to ε_1. In this band, ε_1 is given by the equation [44–46]:

$$\varepsilon_1 = 1 + \omega_p^2 \sum \frac{f_n}{(\omega_n^2 - \omega^2)}, \quad (16)$$

where f_n is the oscillator strength corresponding to the transition dipole at frequency ω_n. In the framework of the single oscillator model, we consider a single oscillator which has angular frequency ω_0 (energy E_0) and therefore neglect the effect of the others. In the spectral study, it can be limited to a single oscillator, which has the most dominant contribution and whose strength is denoted as f_0. Then the relationship can be reduced by introducing energy parameters E_0 and E_d to the equation [47,48]:

$$n^2 = 1 + \frac{E_0 E_d}{E_0^2 - E^2}, \quad (17)$$

where $E = h\nu$ is the incident photon energy, E_0 the single-oscillator energy and E_d the dispersion energy. The variation of $(n^2-1)^{-1}$ *vs.* $(h\nu)^2$ allows us to reach E_0 and E_d constants. Their values are listed in table 8.

It is found that values of both Cauchy and Wemple Di-Dominoco parameters are strongly dependent on europium doping level. Furthermore, dispersive energy (E_d) has a minimum ~12.5 eV for 1% doping level. This level seems good by reducing the response dispersion of solar cells using such doping material.

3.2d *Complex dielectric functions*: The fundamental electron excitation spectrum of the films is described by using

a frequency dependence of the complex electronic dielectric constant. The dielectric constant is defined as

$$\begin{cases} \varepsilon(\lambda) = (n(\lambda) - ik(\lambda))^2 = \varepsilon_1(\lambda) - i\varepsilon_2(\lambda), \\ \begin{cases} \varepsilon_1(\lambda) = n(\lambda)^2 - k(\lambda)^2, \\ \varepsilon_2(\lambda) = 2n(\lambda)k(\lambda). \end{cases} \end{cases} \tag{18}$$

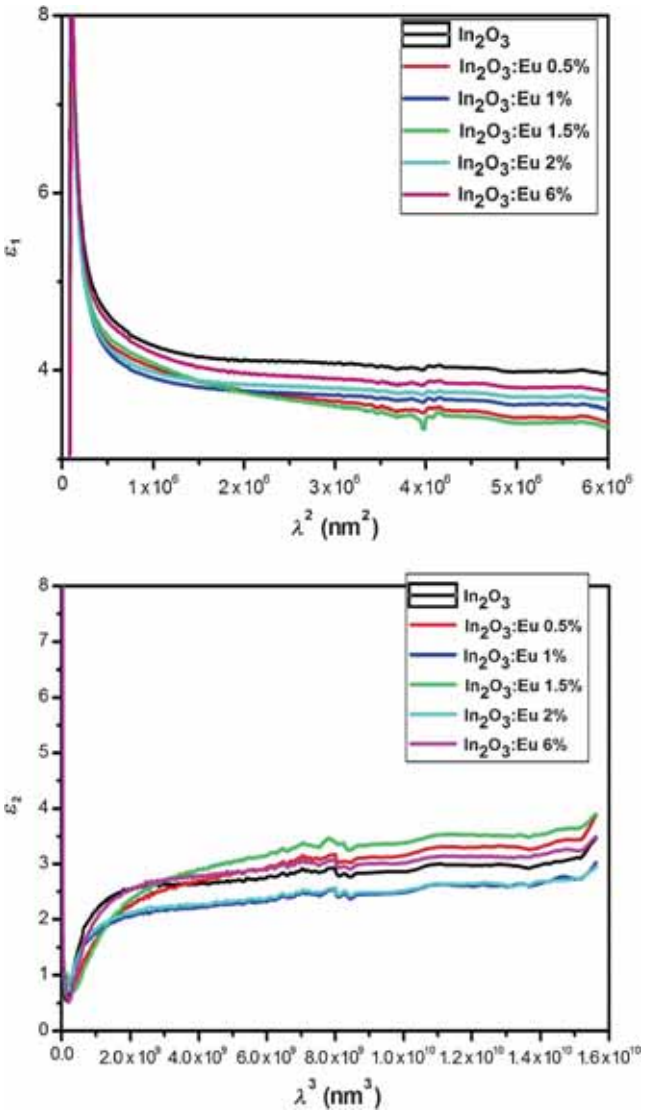

Figure 8. Variation of the real part with λ^2 and imaginary part with λ^3 of complex dielectric constant of Eu-doped In_2O_3 thin films.

Table 9. Optical constants of Eu-doped In_2O_3 thin films.

	ε_∞	ω_p (10^{14} rad s^{-1})	τ (10^{-16} s)
In_2O_3	4.201	1.907	5.786
In_2O_3 : Eu 0.5%	3.974	3.078	7.543
In_2O_3 : Eu 1%	3.876	2.220	5.980
In_2O_3 : Eu 1.5%	4.141	3.957	1.275
In_2O_3 : Eu 2%	3.938	2.056	5.447

For all samples, it is found that in infrared range ε_1 is linear function of the square of the wavelength (figure 8), while ε_2 is practically linear with λ^3. This behaviour was used to evaluate ε_∞, ω_p and τ, high frequency dielectric constant, plasma frequency and relaxation time, respectively, through the relations:

$$\begin{cases} \varepsilon_1 \approx \varepsilon_\infty - \dfrac{\varepsilon_\infty \omega_p^2}{4\pi^2 c^2}\lambda^2 \\ \varepsilon_2 = 2nk \approx \dfrac{\varepsilon_\infty \omega_p^2}{8\pi^3 c^3 \tau}\lambda^3 \\ \omega_p^2 = \dfrac{4\pi Ne^2}{\varepsilon_\infty m_e^*} \end{cases} \tag{19}$$

where N/m_e^* represents free carriers concentration-to-effective mass ratio. Calculated values of ε_∞, ω_p, τ and N/m_e^* are given in table 9.

From this study, it is shown that the high plasma pulsation (ω_p) has a maximum value at 1.5 at% doping level which indicates a high interaction with optical radiation.

3.3 *Vibrational study by Raman spectroscopy analysis*

Additional information on the structure of the sample was obtained by Raman spectroscopy. Figure 9 depicts the thin Raman spectra of the as-grown single crystalline In_2O_3. It is well known that cubic In_2O_3 structure belongs to the I_a^3, T_h^7 space group. For such structure, the vibrations with symmetry A_g, E_g and T_g are Raman active and T_u vibrations are IR active; in fact, 22 Raman-active and 16 infra-red active modes are expected but only 6 Raman modes and 11 IR modes were previously detected as truly In_2O_3 cubic modes [20,21]. The In_2O_3 spectrum shows (figure 9) the expected vibrational modes at 106, 131, 305 and 366 cm^{-1}, which are the signatures of the cubic In_2O_3 structure [22]. Also, figure 9 shows that the highest intensity of Raman peaks are obtained for In_2O_3 : Eu 1.5 at%.

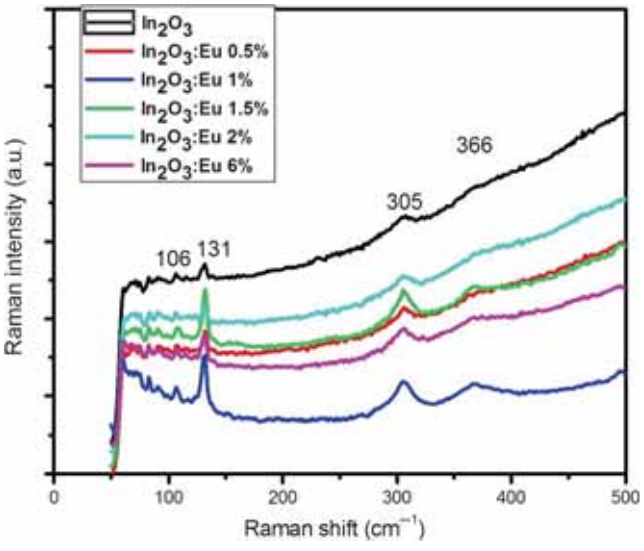

Figure 9. Raman spectra of Eu-doped In_2O_3 thin films.

3.4 *Photoluminescence*

The photoluminescence spectra of the as-grown, oxidized and deoxidized of the In_2O_3 were measured under the excitation at 350 nm. Figure 10a shows the PL spectrum obtained from the as-grown In_2O_3. The peak centred at 394 nm must be originated from the free exciton emission around 3.14 eV from the wide-band-gap In_2O_3. The stable blue light was also observed at 423, 436 and 487 nm. A strong and broad PL emission spectrum recorded from the In_2O_3 nanofibres is reported with its maximum intensity centred at 470 nm [49]. It is reported that the In_2O_3 nanowires have PL peaks centred at 425, 429, 442, 460 nm [50], 398 nm [51], 416 and 435 nm [52]. The nanocubes have a strong PL peak centred at 450 nm [53,54].

The photoluminescence peaks in the visible emission would be attributed to the oxygen vacancies.

3.5 *Photocatalytic activity test*

Photocatalytic activities were evaluated by the degradation of an organic dye, methylene blue (MB), in an aqueous solution under ultraviolet light irradiation for 1 h. The UV light was obtained using a lamp (Northen Electronic, Wigan, Lancs). A volume of 30 ml of aqueous solution of MB (3 mg l^{-1}) was placed in a vessel, and a In_2O_3 : Eu film photocatalyst with the area of 4/4 cm^2 was placed into the solution. Prior to irradiation, the solution was magnetically stirred in the dark for 30 min to establish an adsorption–desorption equilibrium. MB decomposition testing with and without In_2O_3 films for different races of doping were carried out using UV–Vis absorption spectra, as shown in figure 11. It is well known that the most observed absorption peak of MB solution is at 660 nm, which is attributed to that of its monomer [30]. Figure 11 indicates that samples with cubic phase presented higher intrinsic activities for the photodegradation of MB as compared to samples in rutile one.

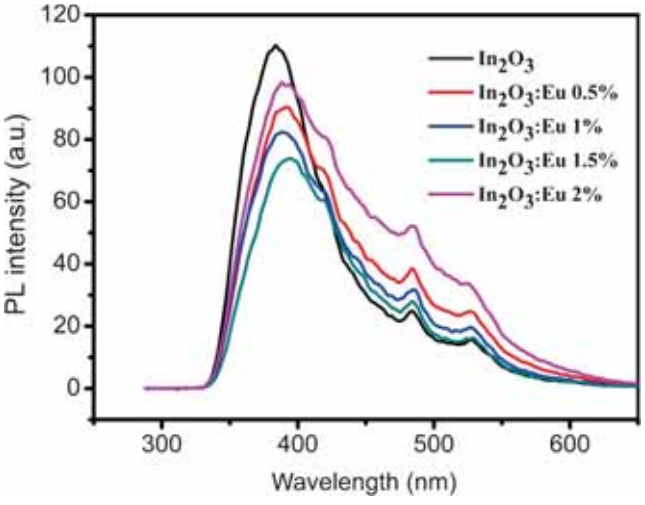

Figure 10. PL spectra of Eu-doped In_2O_3 thin films.

3.6 *Electrical study*

Plots of ln (σ) *vs.* 1000/T of Eu-doped In_2O_3 films are shown in figure 12. The temperature dependence of conductivity shows two different regions (I and II) and the existence of two types of behaviours depending on the doping level. The electrical conductivity increases with temperature. As the temperature increases, more charge carriers overcome the activation energy barrier and participate in the electrical conduction. The electrical conductivity of In_2O_3 : Eu films can be analysed by the following equation:

$$\sigma = \sigma_0 \exp\left(-\frac{E_a}{kT}\right), \tag{20}$$

where σ_0 is constant, k Boltzmann constant and E_a the activation energy.

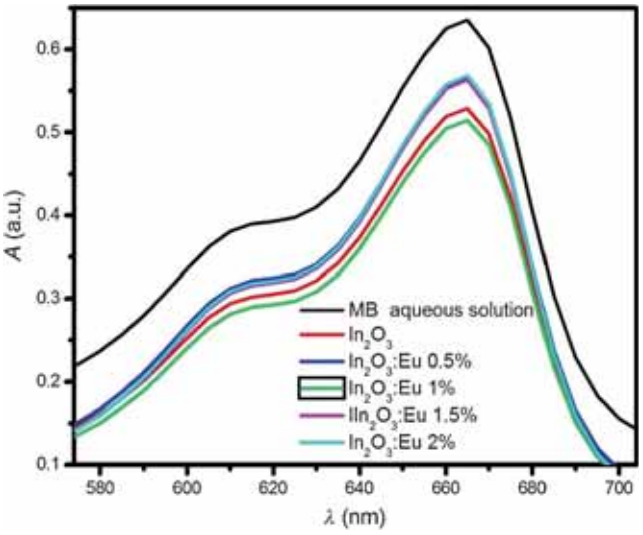

Figure 11. Absorbance spectra of both MB solution and Eu-doped In_2O_3 thin films.

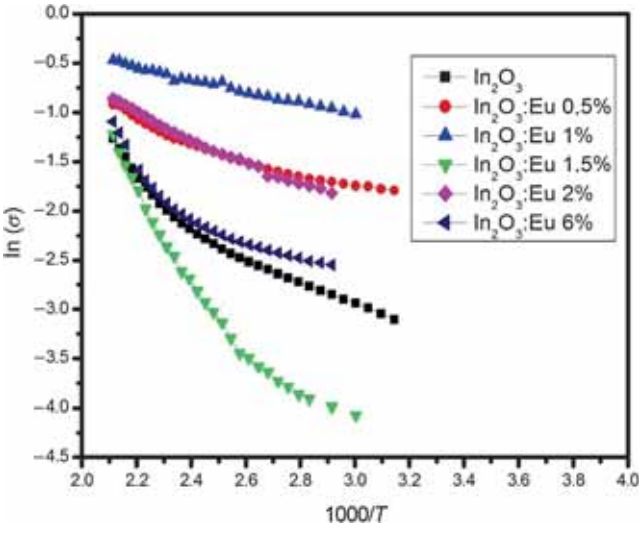

Figure 12. Electrical conductivity as a function of the temperature of Eu-doped In_2O_3 thin films.

The activation energy represents the location of trap levels below conduction band. Activation energy (E_a) values for I and II regions were calculated from the linear portions of figure 12 and listed in table 10. These activation energies indicate the presence of two donor levels: a shallow donor level corresponding to E_a(I) and a deep donor level assigned to E_a(II).

3.7 *Opto-thermal investigation*

The effective absorptivity $\hat{\alpha}$, as defined in precedent studies [55–58], is the mean normalized absorbance weighted by $I(\tilde{\lambda})_{AM1.5}$, the solar standard irradiance:

$$\begin{cases} \hat{\alpha} = \dfrac{\int_0^1 I(\tilde{\lambda})_{AM1.5} \times \alpha(\tilde{\lambda}) d\tilde{\lambda}}{\int_0^1 I(\tilde{\lambda})_{AM1.5} d\tilde{\lambda}}, \\ \begin{cases} \lambda \in [\lambda_{min}, \lambda_{max}] \Leftrightarrow \tilde{\lambda} \in [0, 1], \\ \lambda_{min} = 300 \text{ nm}; \ \lambda_{max} = 1800 \text{ nm}, \end{cases} \end{cases} \quad (21)$$

where $I(\tilde{\lambda})_{AM1.5}$ is the reference solar spectral irradiance fitted using the Boubaker polynomials expansion scheme (BPES) [59–71]:

$$I(\tilde{\lambda}) = \left[\frac{1}{2N_0} \sum_{n=1}^{N_0} \theta_n . B_{4n}(\tilde{\lambda} \times \beta_n) \right],$$

where β_n are the Boubaker polynomials [61–69], B_{4n} minimal positive roots, θ_n the given coefficients, N_0 a given integer, $\alpha(\tilde{\lambda})$ the normalized absorbance spectrum and $\tilde{\lambda}$ the normalized wavelength.

The normalized absorbance spectrum $\alpha(\tilde{\lambda})$ is deduced from the BPES by establishing a set of N experimental measured values of the transmittance–reflectance vector $\left(T_i(\tilde{\lambda}_i); R_i(\tilde{\lambda}_i)\right)\Big|_{i=1...N}$ *vs.* the normalized wavelength $\tilde{\lambda}_i\Big|_{i=1...N}$.

Then the system (22) is set as:

$$\begin{cases} R(\tilde{\lambda}) = \left[\dfrac{1}{2N_0} \sum_{n=1}^{N_0} \xi_n \times B_{4n}(\tilde{\lambda} \times \beta_n) \right], \\ T(\tilde{\lambda}) = \left[\dfrac{1}{2N_0} \sum_{n=1}^{N_0} \xi_n' \times B_{4n}(\tilde{\lambda} \times \beta_n) \right], \end{cases} \quad (22)$$

where β_n are the $4n$-Boubaker polynomials, B_{4n} minimal positive roots [63–66], N_0 a given integer and ξ_n and ξ_n' the coefficients determined through the Boubaker polynomials expansion scheme (BPES).

The normalized absorbance spectrum $\alpha(\tilde{\lambda})$ is deuced from the relation:

$$\alpha(\tilde{\lambda}) = \frac{1}{d\sqrt[4]{2}} . \sqrt[4]{\left(\ln \frac{1 - R(\tilde{\lambda})}{T(\tilde{\lambda})} \right)^4 + \left(2 \ln \frac{1 - R(\tilde{\lambda})}{\sqrt{T(\tilde{\lambda})}} \right)^4}, \quad (23)$$

where d is the layer thickness.

The obtained value of normalized absorbance spectrum $\alpha(\tilde{\lambda})$ is a final guide to the determination of the effective absorptivity $\hat{\alpha}$ through equation (21).

The Amlouk–Boubaker opto-thermal expansivity ψ_{AB} is a thermo-physical parameter defined in precedent studies [72,73], as a 3D expansion velocity of the transmitted heat inside the material. It is expressed in $m^3\ s^{-1}$, and calculated by:

$$\Psi_{AB} = D/\hat{\alpha}, \quad (24)$$

where D is the thermal diffusivity and $\hat{\alpha}$ the effective absorptivity, which is obtained from experimental absorbance spectra. Values of the Amlouk–Boubaker opto-thermal expansivity ψ_{AB} of the studied films are given in table 11.

As observed in subsection 3.1, 3.2c and 3.5, a confirmed enhancement of the opto-thermal response of the doped samples occurred with low Eu incorporation levels (about 0.5%). According to precedent investigations, higher Eu doping ratio causes this enhancement to diminish again in this experiment.

3.8 *Lattice compatibility theory investigation*

The lattice compatibility theory, as mentioned in some recent studies [74–77] is based on the interaction of doping-element lattice behaviour *vs.* host edifice.

Table 10. Activation energy values of Eu-doped In_2O_3 thin films.

	E_A (meV) region I, high temperature	E_A (meV) region II, low temperature
In_2O_3	263	92
In_2O_3 : Eu 0.5%	120	41
In_2O_3 : Eu 1%	60	45
In_2O_3 : Eu 1.5%	367	119
In_2O_3 : Eu 2%	128	74

Table 11. Values of the Amlouk–Boubaker opto-thermal expansivity ψ_{AB} of thin films.

Sample	Pure In_2O_3	In_2O_3 : Eu 0.5%	In_2O_3 : Eu 1.0%	In_2O_3 : Eu 1.5%	In_2O_3 : Eu 2.0%
ψ_{AB} (10^{-12} $m^3\ s^{-1}$)	4.429	1.486	2.045	3.532	4.119

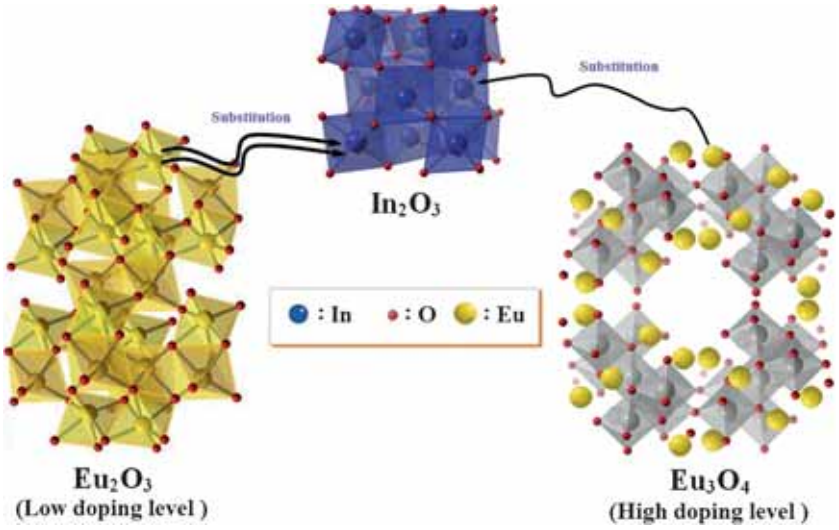

Figure 13. Lattice compatibility theory synoptic scheme for the Eu-doped films.

Preludes to this theory have been established by Boubaker *et al* [74–76] in the context of analysing Urbach tailing controversial behaviour in some nanocompounds as well as I–III–O_2 ternary oxides instability at low temperatures. It was also confirmed by Petkova *et al* [74] on the bases of investigation on some copper-doped compounds. An original formulation of the lattice compatibility theory [77] has been established as following:

> '*The stability of doping agents inside host structures is favorized by geometrical compatibility, expressed in terms of matching patterns between doping agent intrinsic lattice and those of the host*'.

In the actually discussed case (pure and Eu-doped In_2O_3), the nature of highest occupied bands as well as the location of the reciprocal ions Eu^{3+} upper level ($^5D_0$) and eventually ($^7F_2$) within In_2O_3 lattice structures have been demonstrated to be determinant. In this context, fundamental geometrical observations concerning the structure of intrinsic europium oxide, Eu_2O_3 lattice along with that the host matrix, In_2O_3 (figure 13) were interpreted in terms of conventional lattice-linked parameters (lattice parameters, bond spatial extent, configurations and angles). Similarities between the two structures pled in favour of an easy substitution process between Eu ions and those of indium. This substitution is likely to be regulated by doping excess, which may yield the higher degree oxide Eu_2O_3. In fact, high amounts of europium may re-establish the duality of stronger acceptors Eu^{3+} ($^5D_0$) which recovers host lattice initial stability. This last fact, which resulted in less europium incorporation, can justify the recession of some properties for doping amount around 1.0% as noticed in subsections 3.1, 3.2c and 3.5.

Further, and as stated by Souriau *et al* [78] and Kudrawiec *et al* [79], europium doping effects have been recorded to be relevant only at low levels. By analogy and along with lattice compatibility theory, lattice compatibility theory (LCT) patterns, an explanation to the irregular incorporation of europium in the targeted matrix by occupying In ions place can be given. Indeed, optimality, in the sense of photoluminescence or optical efficiency, which was detected at around 1.0% of doping rate, needs more thorough investigation.

4. Conclusion

Indium oxide thin films were prepared with various europium doping concentrations using spray pyrolysis method. The structural and optical properties were discussed in terms of Eu content. Far from common characterization means that the work was focussed on PL and electrical conductivity performances due to the emergence of related application fields.

LCT analyses led to a plausible explanation of some recorded irregularities in europium element incorporation within In_2O_3 cubic lattice. Optimality, in the sense of structural and optical efficiencies, has been detected and delimited at around 1% of doping rate. This work may be of interest since a simple method is used to prepare Eu-doped In_2O_3 thin films, which is very promising and is subsequently a great potential in the field of optoelectronics as well as in sensitivity devices.

References

[1] Wang G, Park J, Wexler D, Parkv Sik and Ahn J-H 2007 *Inorg. Chem.* **46** 4778
[2] Mi Y, Odoka H I and Iwata S 1999 *Jpn. J. Appl. Phys.* **38** 3453
[3] Martha S, Hemalata Reddy K and Parida K M 2014 *J. Mater. Chem. A* **2** 3621
[4] Ginley D and Bright C 2000 *MRS Bull.* **25** 15
[5] Cantalini C, Wlodarski W, Sun H T, Atashbar M Z, Passacantando M, Phani A R and Santucci S 1999 *Thin Solid Films* **350** 276
[6] Liang C, Meng G, Lei Y, Phillipp F and Zhang L 2001 *Adv. Mater.* **13** 1330

[7] Kolmakov A I and Moskovits M 2004 *Rev. Mater. Res.* **34** 151

[8] Jeffrey W Elam, Alex B F Martinson, Michael J Pellin and Joseph T Hupp 2006 *Chem. Mater.* **18** 3571

[9] Chen T P, Shih H Y, Lian J T, Chen J H, Lin P S, Lin T Y *et al* 2012 *Opt. Exp.* **20** 17136

[10] Arshak K, Moore E, Lyons G M, Harris J and Clifford S 2004 *Sens. Rev.* **24** 181

[11] Flueckiger J, Ko K and Cheung K C 2009 *Sensors* **9** 9196

[12] Zang W, Yuxin Nie, Dan Zhu, Ping Deng, Lili Xing and Xinyu Xue 2014 *J. Phys. Chem. C* **118** 9209

[13] Li E, Cheng Z, Xu J, Pan Q, Yu W and Chu Y 2009 *Cryst. Growth Des.* **9** 2146

[14] Zhou H, Cai W and Zhang L 1999 *Mater. Res. Bull.* **34** 845

[15] Yang H, Zhang X and Tang A 2006 *Nanotechnology* **17** 2860

[16] Ayeshamariam A, Bououdina M and Sanjeeviraja C 2013 *Mater. Sci. Semicond. Process.* **16** 686

[17] Von Graberg T, Hartmann P, Rein A, Gross S, Seelandt B, Röger C *et al* 2011 *Sci. Technol. Adv. Mater.* **12** 025005

[18] Gao J, Chen R, Li D H, Jiang L, Ye J C, Ma X C *et al* 2011 *Nanotechnology* **22** 195706

[19] Kim H, Horwitz J S, Kushto G P, Qadri S B, Kafafi Z H and Chrisey D B 2010 *Cryst. Eng. Comm.* **12** 3172

[20] Park C-Y, You C-Y, Jeon K-R and Shin S-C 2012 *Appl. Phys. Lett.* **100** 222409

[21] Sheel D W and Gaskell J M 2011 *Thin Solid Films* **520** 1242

[22] Józefowicz M and Piekarczyk W 1987 *Mater. Res. Bull.* **22** 775

[23] Karthikeyan S, Hill A E and Pilkington R D 2014 *Thin Solid Films* **550** 140

[24] Stern E, Cheng G, Guthrie S, Turner-Evans D, Broomfield E, Lei B *et al* 2006 *Nanotechnology* **17** S246

[25] Fellahi N, Addou M, Sofiani Z, El Jouad M, Bahedi K, Bayoud S *et al* 2010 *J. Optoelectron. Adv. Mater.* **12** 1087

[26] Gurlo A, Ivanovskaya M, Pfau A, Weimar U and Göpel W 1997 *Thin Solid Films* **307** 288

[27] Liu J, Wu D and Zeng S 2009 *J. Mater. Process. Technol.* **209** 3943

[28] White W B and Keramidas V G 1972 *Spectrochim. Acta A* **28** 501

[29] Wang C Y, Dai Y, Pezolt J, Lu B, Kups T, Cimalla V and Ambacher O 2008 *Cryst. Growth* **8** 1257

[30] Sobotta H, Neumann H, Kuhn G and Riede V 1990 *Cryst. Res. Technol.* **25** 6

[31] Liu J, Wu D and Zeng S 2009 *J. Mater. Process. Technol.* **209** 3943

[32] Prathap P, Subbaiah Y P V, Devika M and Ramakrishna Reddy K T 2006 *Mater. Chem. Phys.* **100** 375

[33] Ben Amor M, Boukhachem A, Boubaker K and Amlouk M 2014 *Mater. Sci. Semicond. Process.* **27** 994

[34] Tripathi R, Kumar A, Bharti C and Sinha T P 2010 *Curr. Appl. Phys.* **2** 676

[35] Junaid S, Qazi S, Rennie A R, Cockcroft J K and Vickers M 2009 *J. Colloid Interf. Sci.* **1** 105

[36] El-Nahass M M, Farag A A M, Ibrahim E M and Abd-el-Rahman S 2004 *Vacuum* **72** 453

[37] Boukhachem A, Ouni B, Karyaoui M, Madani A, Chtourou R and Amlouk M 2012 *Mater. Sci. Semicond. Process.* **15** 282

[38] Boukhachem A, Bouzidi C, Boughalmi R, Ouerteni R, Kahlaoui M, Ouni B *et al Ceram. Inter.* **40** 13427

[39] Li X Y, Li H J, Wang Z J, Xia H, Xiong Z Y and Wang J X 2009 *Opt. Commun.* **282** 247

[40] Pankove J I 1971 *Optical processes in semiconductors* (Englewood Cliffs, NJ: Prentice-Hall Inc.)

[41] Mott N F and Davis E A 1979 *Electronics processes in non-crystal materials* (Oxford: Clarendon Press) p 428

[42] Bathe R and Patil P S 2007 *Solar Energy Mater. Solar Cells* **91** 1097

[43] Belgacem S and Bennaceur R 1990 *Rev. Phys. Appl. (Paris)* **25** 1245

[44] Segall B and Marple D T F 1967 *Intrinsic exciton absorption*, in *Physics and chemistry of II–VI compounds* (eds) Aven M and Prener J S (Amsterdam: North-Holland) p 319

[45] Altarelli M and Lipari N O 1977 *Phys. Rev. B* **15** 4898

[46] Yu P Y 1979 *Comm. Solid State Phys.* **9** 37

[47] Di-Domenico Jr M, Eibschütz M, Guggenheim H J and Camlibel I 1969 *Solid-State Commun.* **16** 1119

[48] Wemple S H 1973 *Solid-State Commun.* **12** 701

[49] Liang C, Meng G, Lei Y, Phillipp F and Zhang L 2001 *Adv. Mater.* **13** 1330

[50] Zheng M J, Zhang L D, Li G H, Zhang X Y and Wang X F 2001 *Appl. Phys. Lett.* **79** 839

[51] Cao H, Qiu X, Liang Y, Zhu Q X Y and Zhao M 2003 *Appl. Phys. Lett.* **83** 761

[52] Wu X C, Hong J M, Han Z J and Tao Y R 2003 *Chem. Phys. Lett.* **373** 28

[53] Tang Q, Zhou W, Zhang W, Ou S, Jiang K, Yu W and Qian Y 2005 *Cryst. Growth Design* **5** 147

[54] Wu P, Li Q, Zou X N, Cheng W, Zhang D and Zhao C 2009 *J. Phys.: Conf. Ser.* **188** 012054

[55] Amlouk A, Boubaker K and Amlouk M 2010 *J. Alloys Compd.* **490** 602

[56] Amlouk A, Boubaker K, Amlouk M and Bouhafs M 2009 *J. Alloys Compd.* **485** 887

[57] Oyodum O D, Awojoyogbe O B, Dada M and Magnuson J 2009 *Euro. Phys. J. Appl. Phys.* **46** 21201

[58] Awojoyogbe O B and Boubaker K 2009 *Curr. App. Phys.* **9** 278

[59] Ghanouchi J, Labiadh H and Boubaker K 2008 *Int. J. Heat Tech.* **26** 49

[60] Slama S, Bessrour J, Bouhafs M and Ben Mahmoud K B 2009 *Num. Heat Transf. Part A* **55** 401

[61] Slama S, Bouhafs M and Boubaker K 2008 *Int. J. Heat Tech.* **26** 141

[62] Slama S, Bessrour J, Boubaker K and Bouhafs M 2008 *Eur. Phys. J. Appl. Phys.* **44** 317

[63] Slama S, Bessrour J, Boubaker K and Bouhafs M 2008 *Proc. COTUME'08* 79

[64] Fridjine S and Amlouk M 2009 *Modern Phys. Lett. B* **23** 2179

[65] Fridjine S, Boubaker K and Amlouk M 2009 *Canad. J. Phys.* **87** 653

[66] Fridjine S, Mahmoud K B, Amlouk M and Bouhafs M 2009 *J. Alloys Compd.* **479** 457

[67] Tabatabaei S, Zhao T, Awojoyogbe O and Moses F 2009 *Heat Mass Transf.* **45** 1247

[68] Belhadj A, Onyango O and Rozibaeva N 2009 *J. Thermophys. Heat Transf.* **23** 639

[69] Labiadh H 2007 *J. Diff. Eq. C. Proc.* **1** 172

[70] Boubaker K 2007 *Trends Appl. Sci. Res.* **2** 540

[71] Ben Mahmoud K B 2009 *J. Thermoph. Heat Transf.* **23** 409

[72] Amlouk A, Boubaker K and Amlouk M 2010 *J. Alloys Compd.* **490** 602

[73] Amlouk A, Boubaker K, Amlouk M and Bouhafs M 2009 *J. Alloys Compd.* **485** 887

[74] Boubaker K 2012 *ISRN Nanomaterials* **2012** 4

[75] Boubaker K 2013 *J. Ceram.* **2013** 6

[76] Boubaker K, Amlouk M, Louartassi Y and Labiadh H 2013 *J. Aust. Ceram. Soc.* **49** 115

[77] Petkova P and Boubaker K 2013 *J. Alloys Compd.* **546** 176

[78] Souriau J-C, Jiang Y D, Penczek J, Paris H G and Summers C J 2000 *Mater. Sci. Eng. B* **76** 165

[79] Kudrawiec R, Podhorodecki A, Mirowska N, Misiewicz J, Molchan I, Gaponenko N V, Lutich A A and Gaponenko S V 2003 *Mater. Sci. Eng. B* **1055** 53